https://doi.org/10.5194/amt-2021-272
Preprint. Discussion started: 21 September 2021

Atmospheric Measurement Techniques Discussions

Laboratory evaluation of the scattering matrix of ragweed, ash, birch and pine pollens towards pollen classification

Danaël Cholleton[1,2], Émilie Bialic[2], Antoine Dumas[2], Pascal Kaluzny[2], Patrick Rairoux[1], Alain Miffre[1]

[1]University of Lyon, Université Claude Bernard Lyon 1, CNRS, Institut Lumière Matière, F-69622, VILLEURBANNE, France
[2]TERA Sensor, ZI Rousset, 296 Avenue Georges Vacher, 13790, Rousset, France

Correspondence to: Alain Miffre (alain.miffre@univ-lyon1.fr)

Abstract. Pollens are nowadays recognized as one of the main atmospheric particles affecting public human health as well as the Earth's climate. In this context, an important issue concerns our ability to detect and differentiate among the existing pollen taxa. In this paper, the potential differences that may exist in light scattering by four of the most common pollen taxa, namely ragweed, birch, pine and ash, are analysed in the framework of the scattering matrix formalism at two wavelengths simultaneously (532 and 1064 nm). Interestingly, our laboratory experimental error bars are precise enough to show that these four pollens, when embedded in ambient air, exhibit different spectral and polarimetric light scattering characteristics, in the form of ten scattering matrix elements (five per wavelength), which allow identifying each separately. To end with, a simpler light scattering criterion is proposed for classifying among the four considered pollens by performing a principal component (*P*C) analysis, that still accounts for more than 99 % of the observed variance. We thus believe this work may open new insights for future atmospheric pollen detection.

1 Introduction

Pollen are biological aerosols impacting public health (Schaffner et al., 2020) and the Earth's climate (Li et al., 2013). The economical cost of pollen allergy on public health is impressive and has been estimated to reach up to 151 billion euros in Europe in 2014 (Lake et al., 2017). Moreover, this cost is expected to increase as the prevalence of allergies in the global population is increasing worldwide. Apart from this socio-economical cost, pollens may locally influence the Earth's radiative forcing, by increasing the IR downwelling flux (Spänkuch et al., 2000) and by acting as cloud-condensation nuclei (Pope, 2010). Indeed, pollen concentrations are expected to increase by 400 % in the following decades (Hamaoui-Laguel et al., 2015) due to climate change, which increases the global temperature and CO_2 atmospheric concentrations while the length of the pollen season should extend. Moreover, the geographical repartition of pollen plants is also expected to extend. These health and climatic impacts mainly depend on the involved pollens species, which are numerous and induce various allergenic reactions. To better quantify the impact of pollens on human health and climate, and as underscored by (Crouzy et al., 2016), reliable measurements and forecasts are required as well as a reliable method for pollen identification and classification. At present, the most widely used methodology is that developed by (Hirst, 1952) seventy years ago, consisting in sampling then

https://doi.org/10.5194/amt-2021-272
Preprint. Discussion started: 21 September 2021


Atmospheric Measurement Techniques Discussions

precipitating atmospheric pollen grains on an adhesive substrate prior to the microscopic observation of the deposited pollen grains. Though rather accurate, this historical methodology suffers from a too long time duration, with characteristic times ranging from a few hours to a week, much higher than the characteristic time for the impact of pollens on human health. Another limitation of the historical methodology is that the pollens grains are counted one by one and identified by a scientist, which is time-consuming and may be operator dependent (Comtois et al., 1999). In this context, deep learning recently improved the identification of pollen grains through microscopy (Daood et al., 2016) by automating the procedure to differentiate among existing pollens. Besides, new methodologies based on interferometry, light-scattering or laser-induced fluorescence have been developed. In the latter, the fluorescence spectrum and its life-time have been used from the UV to the NIR spectral range to identify pollens (Pan et al., 2011; Kiselev et al., 2013). Likewise, image recognition on pollen grains holographic images is also used (Giri et al., 2019; Sauvageat et al., 2020; Kemppinen et al., 2020) as an identification methodology. Finally, light scattering by pollens has been studied in laboratory in aqueous solutions by (Bickel and Stafford, 1980) or when pollens are deposited on a substrate or an holder by (Surbek et al., 2011; Iwai, 2013; Raman et al., 2013; Nouri et al., 2018). Concerning airborne pollens, (Matsuda and Kawashima, 2018; Holler et al., 2016) studied forward and side scattering while polarization-dependent features of light scattering were first studied by our group by evaluating the scattering matrix of ragweed pollen in laboratory ambient air at near backscattering angles (Cholleton et al., 2020). More recently, (Gómez Martín et al., 2021) evaluated the scattering matrix of cypress pollen far from the backscattering angle. Also, the depolarization ratio of several pollens has been studied in field by (Cao, 2010; Bohlmann et al., 2018; Sicard et al., 2021) using lidar measurements. Nevertheless, light scattering by pollens embedded in ambient air still remains a complex topic, mostly due to the complexity in size and shape of the pollen taxa. In particular, it is not a priori granted that pollen differing in size and shape exhibit different light scattering characteristics. Indeed, as underscored in (Cholleton et al., 2020), no analytical light scattering numerical simulation exists for such complex objects so that a remaining issue is to predict how these grains scatter light. Therefore, a controlled-laboratory experiment is coveted to address light scattering by pollens with a precision allowing to identify each pollen.

In this paper, to complement the above airborne pollen studies, the scattering matrix of several airborne pollen taxa is for the first time presented. The four considered pollen taxa are ragweed, ash, birch and pine, chosen for their important impact on human health. The laboratory experiment is carried out at two wavelengths simultaneously ($\lambda_{VIS} = 532$ nm and $\lambda_{IR} = 1064$ nm) and provides five scattering matrix elements per pollen taxa and per wavelength. Interestingly, our experimental error bars are precise enough to reveal the existing differences in light scattering by these four pollens, thus allowing to identify each separately. Ten scattering matrix elements are provided per pollen (five per wavelength). Hence, compared with our previous contribution (Cholleton et al., 2020), three more pollens are here studied (ash, birch and pine) which allows discussing on airborne pollen classification using polarization-resolved light scattering. As an output, a principal component analysis is applied to provide a simpler light-scattering criterion for classifying among these four pollens. The classification can then be visualized on a simple 2D-plane representation. The novelty of the paper is hence two-fold. Firstly, precise light scattering

https://doi.org/10.5194/amt-2021-272
Preprint. Discussion started: 21 September 2021


Atmospheric Measurement Techniques Discussions

characteristics of ragweed, ash, birch and pine are revealed in the form of ten scattering matrix elements (five per pollen per wavelength). Secondly, an analysis is proposed towards a pollen classification. The paper is organised as follows. Section 2 presents the studied pollen samples, by characterizing their size and shape, based on scanning electron microscopic images taken in our laboratory. Section 3 details our laboratory methodology to precisely evaluate the scattering matrix of these pollens by detailing our error uncertainty. Section 4 presents the evaluation of the scattering matrix of ragweed, ash, birch and pine, and proposes the principal component analysis as an outlook as a visual 2D-representation to help classifying among the four considered pollens. The paper ends with a conclusion and proposes outlooks.

2 Pollen samples

Figure 1 shows scanning electron microscopic images of the four studied pollen species, namely ragweed, ash, birch and pine. These microscopic images allow characterizing the size and the shape of these pollens: each pollen exhibits a very characteristic shape with comprising grains presenting a quasi-monodisperse size distribution. The four considered species clearly differ in size and shape, from nearly spherical with a 20 µm volume equivalent diameter for ragweed to highly irregular shapes with a diameter larger than 60 µm for pine. Small-scale features exist at each pollen surface, such as granularity or apertures, which show the great complexity of these microscopic objects. These specific sizes and shapes are used for pollen recognition as extensively detailed in palynological databases (PalDat, 2021), as recalled in the introduction.

2.1 Ragweed

Ragweed or *Ambrosia artemisiifolia* pollen is amongst the most allergenic pollen in Europe and Northern America (Smith et al., 2013) with 15.8 million persons sensitized in Europe (Schaffner et al., 2020). Ragweed pollen induces particular allergenic reactions twice more often as other pollens (Thibaudon et al., 2014) with an annual economic cost of 7 billion euros in Europe (Schaffner et al., 2020). The ragweed season usually lasts from August to October and this duration is getting longer with expected increasing mean temperatures. Hence, ragweed pollen has been extensively studied in the literature (Smith et al., 2013; Hamaoui-Laguel et al., 2015; Zink et al., 2017) and extensive efforts are made for the observations and forecasts of its concentration (Prank et al., 2013). Ragweed pollen grains exhibit a characteristic shape, that bears some resemblance with coronavirus virions (Petrov, 2020), are nearly but non spherical, with a mean volume-equivalent diameter of 21 micrometres. Its membrane exhibit three apertures (2 micrometres long), regular spikes (*echinus)* of about 1 micrometre length and a perforate structure, i.e. covered with holes of about 100 nanometres diameter.

2.2 Ash

Ash (*fraxinus americana*) pollen is a relevant source of allergenic reactions in Europe (Imhof et al., 2014) which has been underestimated for a long time as its bloom season overlap with that of birch. Moreover, it presents a high cross-reactivity from allergens from other plant species (Niederberger et al., 2002). Its blooming season lasts from March to May. Ash pollen

https://doi.org/10.5194/amt-2021-272
Preprint. Discussion started: 21 September 2021

Atmospheric Measurement Techniques Discussions

grains have an irregular shape, with a reticulate exine, i.e. ornamental elements arranged as a network of ridges with gaps of the micron scale, and 3 *colpi*, i.e. thin elongated apertures regularly distributed along its equatorial region. Its volume equivalent diameter is about 31 micrometres.

2.3 Birch

Alongside with ragweed, birch (*betula pendula*) pollen is one of the most impacting in Europe (Biedermann et al., 2019). It also exhibits a cross-reactivity with other allergens. Depending on its location, the birch pollen season starts from March and lasts until late June. Birch pollen grains are irregularly shaped, with sunken interpectoral areas when dried. Their mean volume equivalent diameter is about 28 to 29 micrometres. They present 3 protruding pores, i.e. three 2 µm large holes on its polar view. Birch pollen has been one off the first to be integrated in global pollen forecasts (Siljamo et al., 2013), using dispersion models.

2.4 Pine

In contrary to the previous taxa, pine (*pinus strobus*) pollen rarely cause allergies. It however remains an interesting study case, as it may impact the Earth's climate locally: (Spänkuch et al., 2000) reported that a high pine pollen concentration increased the down welling infrared flux up to 8 times the monthly means. Moreover, this pollen has been studied by optical diffraction tomography (Kim et al., 2018) to highlight its structure and morphological features, and evaluate its refractive index. At last, (Sicard et al., 2021) recently studied its vertical distribution in the atmosphere using lidar-derived profiles. As shown Fig. 1(d), pine pollen is the largest of the studied samples with a mean diameter of 69 micrometers. Its shape largely differs from that of other pollens, as two *sacci*, i.e. two large air-filled bladders are attached to the center part (Schwendemann et al., 2007). The refractive index of pine at 532 nm has been estimated between 1.5 and 1.54 (Kim et al., 2018), while its imaginary part remains undocumented.

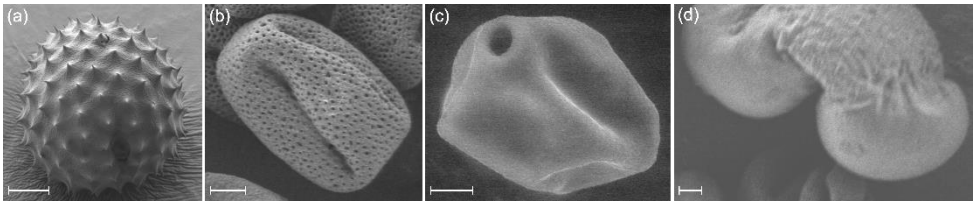

Figure 1 : Scanning electron microscopy (SEM) images of the studied pollens taken at iLM: (a) ragweed (*ambrosia artemisiifolia*), (b) ash (*fraxinus americana*), (c) birch (*betula pendula*), (d) pine (*pinus strobus*). The scale bar is 5 µm on all pictures. Pollen grains were suspended in ambient air and deposited on an adhesive substrate for SEM observations.

2.5 Pollen suspension

The studied pollen samples were supplied by Stallergenes Greer. Dry pollen powder has been suspended in the light scattering volume using a solid aerosol generator supplied with dried compresses air (RH < 10 %). The size distribution and concentration

https://doi.org/10.5194/amt-2021-272
Preprint. Discussion started: 21 September 2021


Atmospheric Measurement Techniques Discussions

of the generated airborne ragweed pollen grains was measured using an Aerodynamic Particle Sizer (APS). As a consistency check, the retrieved ragweed pollen size distribution was found in agreement with the size specified by the supplier and also with above SEM observations issued from the state-of-the-art literature (PalDat, 2021).

3 Methodology

3.1 Light scattering by pollens

We consider elastic light scattering by an ensemble of pollen grains suspended in ambient air with a polarized electromagnetic incident radiation of wavelength λ. For the pollen samples are nonspherical (see Fig. 1), the polarization state of the scattered radiation may differ from that of the incident radiation. To describe the polarization states of the incident and scattered waves, the Stokes vector formalism (Mishchenko et al., 2002) is applied. The polarization state of the incident and scattered radiation is then described by a Stokes vector $S = [I, Q, U, V]^T$ where I, Q, U, V respectively relate to the total intensity, the linear degree of polarization in the scattering plane, and at 45° from it, and the degree of circular polarization. In the far-field single scattering approximation and assuming random orientation, we learn from light scattering textbooks (Mishchenko et al., 2002) that the incident and scattered Stokes vectors $\mathbf{S_0}$ and $\mathbf{S}$ relate by the so-called scattering matrix :

$$\begin{bmatrix} 1 & f_{12}^{\lambda} & 0 & 0 \\ f_{12}^{\lambda} & f_{22}^{\lambda} & 0 & 0 \\ 0 & 0 & f_{33}^{\lambda} & f_{34}^{\lambda} \\ 0 & 0 & -f_{34}^{\lambda} & f_{44}^{\lambda} \end{bmatrix} \quad (1)$$

where the scattering matrix elements f_{ij}^{λ} $(i, j = 1 - 4)$ have been normalized with respect to the scattering phase function so that f_{ij}^{λ} at most equals unity. f_{22}^{λ} and f_{33}^{λ} characterize how a linear polarization state is preserved during light scattering by the considered pollen while f_{44}^{λ} relates if circular polarization is preserved during light scattering by the pollen grains. Off-diagonal element f_{12}^{λ} quantifies the amount of non-polarized light after scattering by pollens, while the other off-diagonal element f_{34}^{λ} traduces the ability of pollens to convert a linearly polarized radiation to a circular polarization state throughout light scattering. The scattering matrix elements describe how the polarization state of the incident radiation is modified during light scattering by the studied pollens grains. These matrix elements hence depend on the shape of the pollen grains which we here investigate.

3.2 Laboratory experimental set-up for pollen light scattering

The specific size and shape of each pollen taxon is addressed by considering the Fig. 2 laboratory experiment, which has proven efficiency for ragweed pollen detection (Cholleton et al., 2020). We here recall its main characteristics for the sake of clarity before discussing on its applicability to the detection of other pollens in the next paragraph. This laboratory polarimeter operates at the near backscattering angle $\theta = (177.5 \pm 0.2)°$ and at two wavelengths $\lambda_{VIS} = 532$ nm and $\lambda_{IR} = 1064$ nm

https://doi.org/10.5194/amt-2021-272
Preprint. Discussion started: 21 September 2021

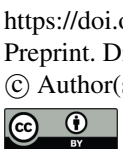

Atmospheric Measurement Techniques Discussions

simultaneously. A reflecting polarizing beam-splitter cube (PBC) is used so that it is the s-component of the scattered radiation that is measured by the photodetector. This experimental set-up has been validated on spherical particles (Cholleton et al., 2020) for which the scattering matrix can be analytically computed by applying the Mie theory, by measuring the corresponding size distribution with particle optical sizers.

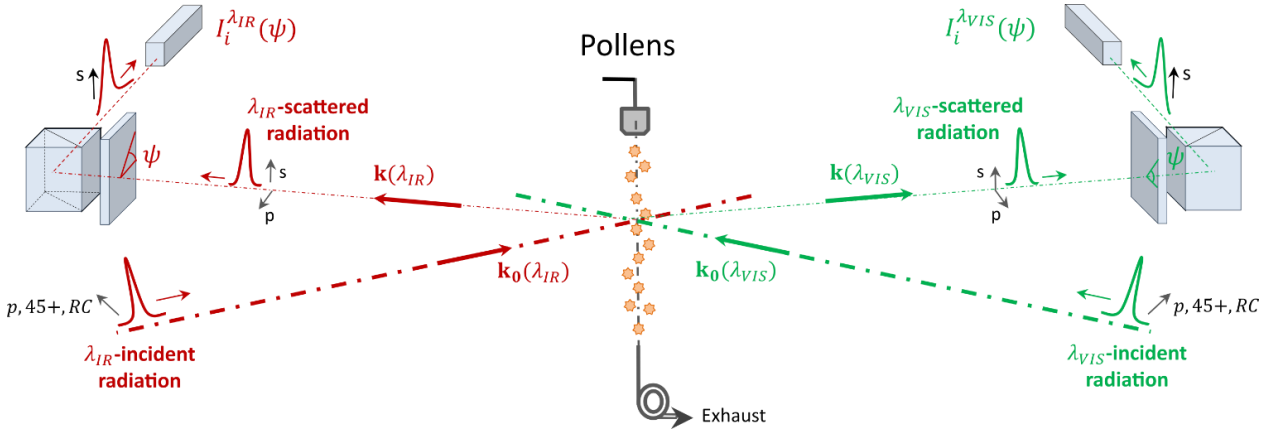

Figure 2: Scheme of the laboratory experimental set-up of the (λ_{VIS}, λ_{IR}) polarimeter from (Cholleton et al., 2020). The 177.5° scattering angle has been exaggerated to ease the reading. $k_0(\lambda)$ and $k(\lambda)$ respectively stand for the incident and scattered wavevectors at wavelength λ. Pollens grains are embedded in laboratory ambient air as described Section 2.5. ψ is the angle between the fast axis of the quarter-wave plate (QWP) and the scattering plane.

Following Fig. 2, the detected pollen scattered intensity can be obtained by considering the successive Mueller matrices encountered by the incident radiation. After a few calculations (Cholleton et al., 2020), , we get at wavelength λ:

$$I_i^{\lambda}(\psi) = I_0^{\lambda} \times \left[a_i^{\lambda} - b_i^{\lambda}\sin(2\psi) - c_i^{\lambda}\cos(4\psi) - d_i^{\lambda}\sin(4\psi)\right] \quad (2)$$

where subscript i stands for incident polarization state while I_0^{λ} is a proportionality constant that accounts for the incident laser power and the electro-optics efficiency. The pollen scattering matrix elements are retrieved from Eq. (2) by adjusting the detected scattered intensity as a function of the angle ψ to retrieve the $a_i^{\lambda}, b_i^{\lambda}, c_i^{\lambda}$ and d_i^{λ} coefficients, which only depend on the scattering matrix elements. To gain in accuracy, the polarization state of the scattered radiation is analysed for several incident polarization states, obtained by rotating an analyser (QWP), whose position is labelled by the angle ψ. To retrieve all the pollen matrix elements, the polarization state of the scattered radiation is analysed for three successive incident polarization states, namely (p), $(45+)$ and (RC). To give an example, a (RC)-polarized incident radiation allows retrieving $f_{12}^{\lambda}, f_{34}^{\lambda}$ and f_{44}^{λ}, as established in (Cholleton et al., 2020). Adding a $(45+)$-polarized incident radiation allows evaluating f_{33}^{λ} in addition. Finally, f_{22}^{λ} is retrieved from a (p)-polarized incident radiation. In summary, the following set of equations, established in (Cholleton et al., 2020), is applied to retrieve the pollen scattering matrix elements from adjusted coefficients $a_i^{\lambda}, b_i^{\lambda}, c_i^{\lambda}$ and d_i^{λ} :

https://doi.org/10.5194/amt-2021-272
Preprint. Discussion started: 21 September 2021

Atmospheric Measurement Techniques Discussions

$$f_{12}^{\lambda} = 2c_{RC}^{\lambda}/(a_{RC}^{\lambda} + c_{RC}^{\lambda}) \quad (3a)$$

$$f_{34}^{\lambda} = 2d_{RC}^{\lambda}/(a_{RC}^{\lambda} + c_{RC}^{\lambda}) \quad (3b)$$

$$f_{44}^{\lambda} = -b_{RC}^{\lambda}/(a_{RC}^{\lambda} + c_{RC}^{\lambda}) \quad (3c)$$

$$f_{33}^{\lambda} = 2d_{45+}^{\lambda}/(a_{45+}^{\lambda} + c_{45+}^{\lambda}) \quad (3d)$$

$$f_{22}^{\lambda} = \left[f_{12}^{\lambda} \times \left(c_p^{\lambda} - a_p^{\lambda}\right) + 2c_p^{\lambda}\right]/\left(a_p^{\lambda} + c_p^{\lambda}\right) \quad (3e)$$

3.3 Applicability of this set-up to the detection of other pollens

To study the sensitivity of our methodology to other pollens, three different Taxa are considered, characterized by the following set of scattering matrix elements:

- a spherical pollen called $Taxon\ 1$, with normalized scattering matrix elements $[f_{22}^{\lambda} = 1, f_{33}^{\lambda} = 1, f_{44}^{\lambda} = -1, f_{12}^{\lambda} = 0, f_{34}^{\lambda} = 0]$. $Taxon\ 1$ is to our knowledge an hypothetical pollen since pollens are nonspherical (Hesse, 2009). It is here however considered for several pollens exhibits an overall spherical shape. Also, the spherical shape is the ideal shape to be detected and can hence be considered as a reference case for polarimetric studies.
- a nonspherical pollen called $Taxon\ 2$ with scattering matrix elements $[f_{22}^{\lambda} = 0.47, f_{33}^{\lambda} = -0.41, f_{44}^{\lambda} = -0.30, f_{12}^{\lambda} = 0.02, f_{34}^{\lambda} = 0.06]$. As to be seen in Section 4, dedicated to our laboratory results, these scattering matrix elements are that of ragweed pollen at wavelength λ_{IR}.
- another nonspherical pollen called $Taxon\ 3$, exhibiting close but different scattering matrix elements compared with $Taxon\ 2$, namely $[f_{22}^{\lambda} = 0.38, f_{33}^{\lambda} = -0.38, f_{44}^{\lambda} = -0.17, f_{12}^{\lambda} = 0.02, f_{34}^{\lambda} = 0.01]$. As to be seen in Section 4, dedicated to our laboratory results, these scattering matrix elements are that of pine pollen at wavelength λ_{IR}.

To fix ideas, we plotted in Fig. 3 the variation of I_i^{λ} as a function of the ψ-angle of the analyser at a given wavelength λ, for $Taxon\ 1, 2, 3$ at the three successive incident polarization states (p), $(45+)$, (RC). Interestingly, each pollen Taxon is associated with a specific light scattering curve, showing the sensitivity of our methodology. From $Taxon\ 1$ to 3, the (p)-polarization curve $I_p^{\lambda}(\psi)$ exhibits varying minima to be related to variations in the f_{22}^{λ}-scattering element. The same conclusions can be drawn with the $I_{RC}^{\lambda}(\psi)$ curve minima, which are determined by the f_{44}^{λ} scattering matrix element. If the $I_{45+}^{\lambda}(\psi)$ curve is π-periodic whatever the considered taxon, its extrema, which depend on $f_{12}^{\lambda}, f_{34}^{\lambda}$ and f_{33}^{λ}, are also Taxon-dependent. As a result, the proposed methodology can potentially be used to differentiate pollens exhibiting different scattering matrix elements. For that however, the scattering matrix elements should be retrieved with precision, as discussed below.

https://doi.org/10.5194/amt-2021-272
Preprint. Discussion started: 21 September 2021

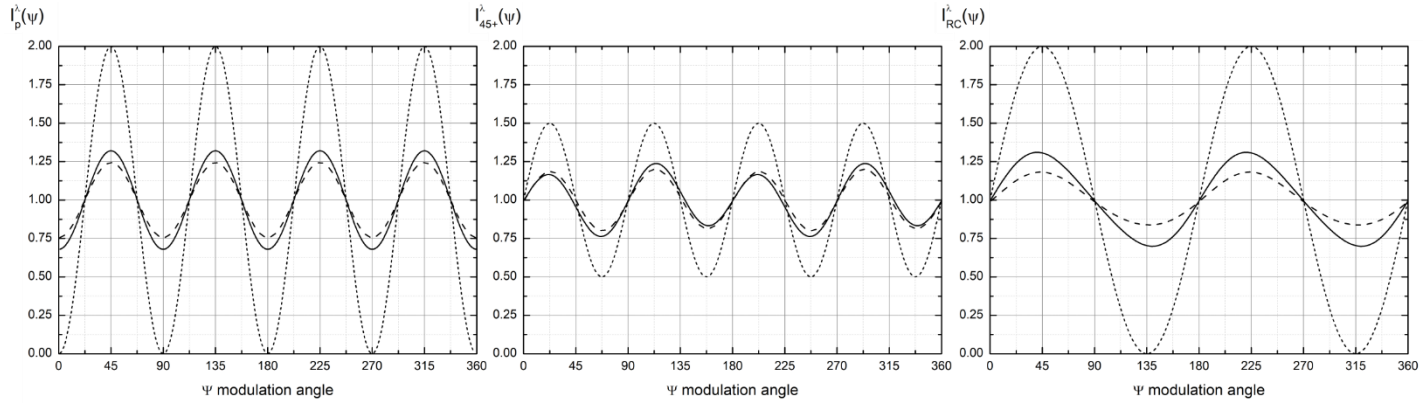

Figure 3: Numerical simulation of the detected scattered light intensity $I_i^\lambda(\psi)$ as a function of the ψ-angle of the analyser for the three considered case studies of pollen taxa : $Taxon$ 1 (dotted lines), $Taxon$ 2 (solid lines), $Taxon$ 3 (dashed lines) at the three successive incident polarization states $(i) = (p), (45+), (RC)$ from left to right. Each curve is normalized to unity (i.e. $I_0^\lambda \times a_i^\lambda = 1$) so that any change in the scattered light intensity be due to polarimetric considerations.

3.4 Scattering matrix elements retrieval accuracy

Taxon 2 can then be distinguished from Taxon 3 using polarimetric light scattering if their corresponding Fig. 3 curves can be distinguished within our experimental error bars. To give an example of our ability to distinguish two pollen taxa, to a 1 %-variation in the f_{44}^λ scattering matrix element corresponds a 1 %-variation in the detected scattered light intensity. For Taxon 2 and 3 exhibit f_{44}^λ –values differing by almost 50 %, the required precision can be reached. Moreover, in our experiment, the evaluation of the $a_i^\lambda, b_i^\lambda, c_i^\lambda$ and d_i^λcoefficients, and hence of the scattering matrix elements (see Eq. 2), relies on a large number of measurements data points (180 points per fitted curve). Special care has indeed been taken to specify our experimental error bars on the retrieved scattering matrix elements by considering both statistical and systematic errors. Polarization cross-talks in the analyser have been minimized by aligning a second polarizing beam-splitter cube in the detector. Wavelength cross-talks are also fully negligible, which is key for revealing the spectral dependence of the scattering matrix elements, for laser-line selective interference filters are used in the light detector. Also, the incident polarization state may slightly differ from the (p), $(45+)$, (RC) polarization states. To quantify this uncertainty, we considered the following incident Stokes vector $S_0 = [1,1,2\chi,2\omega]$, where 2χ and 2ω represent deviations from the (p) incident polarization sate (a similar discussion is drawn for $(45+)$ and (RC) polarization states). At first order in 2χ and 2ω, the uncertainties on the scattering matrix elements $[f_{33}^\lambda, f_{44}^\lambda, f_{12}^\lambda, f_{34}^\lambda]$ are $[2\omega f_{34}^\lambda, 2\chi f_{34}^\lambda, 2\omega f_{22}^\lambda, 2\chi f_{33}^\lambda]$ while the matrix element f_{22}^λ remains unperturbed. As f_{ij}^λ elements at most equal unity, the uncertainties can be majored by their upper limit 2χ or 2ω, depending on the considered scattering matrix element. From a practical point of view, 2χ is evaluated by recording the scattered light intensity by complementary incident polarization states $(45+)$ and $(45-)$. Our calculations indeed show that $2\chi = a_{45+}/(a_{45+} + c_{45+})$- $a_{45-}/(a_{45-} + c_{45-})$.

https://doi.org/10.5194/amt-2021-272
Preprint. Discussion started: 21 September 2021


Atmospheric Measurement Techniques Discussions

Besides, 2ω is evaluated by recording the scattering curve corresponding to incident polarization states (RC) and (LC) since $2\omega = a_{\mathrm{RC}}/(a_{RC} + c_{\mathrm{RC}})$- $a_{\mathrm{LC}}/(a_{\mathrm{LC}} + c_{\mathrm{LC}})$. Finally, we used the outputs of a paper by Mishchenko (Mishchenko et al., 2007) to check that the single scattering approximation was rather safe in our experiment where $k_1\langle d\rangle \gg 30$ (k_1 is the wave vector in the surrounding medium and $\langle d\rangle$ is the average inter-pollen distance), while particle volume concentration remained lower that 1 %, hence considering a tenuous media. Statistical errors due to potential fluctuations in the grain number concentration in the scattering volume are also accounted for by normalizing the detected intensity by that of a photodetector placed at 170°-scattering angle, which depends on the pollen grains number concentration. As a conclusion, from the measurements of the scattered intensity at wavelength λ_{VIS} and λ_{IR}, the above detailed method allows to precisely retrieve the scattering matrix with error bars that are sufficiently low to distinguish pollen Taxa through polarimetric light scattering, as detailed in the Section 4 below, dedicated to our laboratory results.

4 Laboratory results

4.1 Detected scattered light intensity by ragweed, ash, birch and pine

Figure 4 displays the detected scattered light intensity by our four pollen samples (ragweed, ash, birch, pine) at wavelength λ_{VIS} (in green) and λ_{IR} (in red) and at the three incident polarization states (p), $(45+)$, (RC) for a complete rotation of the analyser labelled by the angle ψ. The uncertainty on the incident polarization state has been evaluated by applying the methodology presented in Section 3.4, thus comparing $(45+)$ and (RC) polarization state to their complementary states $(45-)$ and (LC): at both wavelengths, both 2χ and 2ω at most equals 0.01. To minimize statistical errors, each data point results from an average of four measurements each composed of a sequence of 100 laser shots. In Fig. 4, the error bar affecting each data point is then the standard deviation of these four sequences. Moreover, the reproducibility of the observed minima during a full rotation of the analyser indicates that the shape of each considered pollen remained constant during the acquisition. Let us first discuss on the scattered light intensity by ragweed pollen. The (p)-polarization curve exhibits non-zero minima, showing that ragweed pollen grains are non-spherical, in agreement with the SEM observation. In the $(45+)$-polarization curve, the two successive local minima are not equal at wavelength λ_{IR}, which proves that $f_{34}^{\lambda_{IR}}$ is not null, as opposed to wavelength λ_{VIS} where, within our error bars, no significant differences occur in the successive local minima for ragweed for example. Moreover, the light scattering curves differ for the three other pollens (ash, birch, pine). For instance, pine pollen, whose successive local minima are identical in the $(45+)$-polarization curve, exhibits a near zero f_{34}^{λ}-value at both wavelengths as detailed below in Section 4.2. Likewise, the (RC) polarization curve of the ash pollen is nearly constant, which relates to a f_{44}^{λ}-value of the matrix element close to zero.

https://doi.org/10.5194/amt-2021-272
Preprint. Discussion started: 21 September 2021


Atmospheric Measurement Techniques Discussions

4.2 Retrieved scattering matrix elements for ragweed, ash, birch and pine

The Fig. 4 experimental data points are adjusted with Eq. (2) to retrieve the coefficients a_i^λ to d_i^λ (see Fig. 4 fitted curves). The agreement between our measurement data points and the Eq. (2) adjustment is notable. Therefore, we can apply the scattering matrix formalism to evaluate f_{ij}^λ at each wavelength by applying Eqs. (3), as presented in Fig. 5 with detailed numerical values given in Table 1 (wavelength λ_{VIS}) and in Table 2 (wavelength λ_{IR}). We first focus on the comparison of retrieved $f_{ij}^{\lambda_{VIS}}$ between the four pollens before discussing on the spectroscopic variations of these matrix elements. For our four pollens are nonspherical, all the retrieved $f_{22}^{\lambda_{VIS}}$-values differ from unity. More interestingly, within our experimental error bars, each pollen exhibits a different $f_{22}^{\lambda_{VIS}}$ matrix element. Likewise, within our error bars, other diagonal matrix elements $f_{33}^{\lambda_{VIS}}$ and $f_{44}^{\lambda_{VIS}}$, which are also not null and differ from one to another, specifically describe light scattering by each pollen. The $f_{44}^{\lambda_{VIS}}$ element is clearly higher for ragweed and birch, compared with ash and pine. Hence, among our set of four pollens, a set of $f_{ij}^{\lambda_{VIS}}$ elements can be unequivocally linked to a single pollen taxon. Off-diagonal elements $f_{12}^{\lambda_{VIS}}$ and $f_{34}^{\lambda_{VIS}}$ are nearly equal to zero within our error bars. Regarding now wavelength λ_{IR}, the same conclusions can be drawn with $f_{22}^{\lambda_{IR}}$, $f_{33}^{\lambda_{IR}}$ and $f_{44}^{\lambda_{IR}}$, i.e. this set of matrix elements unequivocally relates to a single pollen taxon. Interestingly, while $f_{12}^{\lambda_{IR}}$ remains near-zero, $f_{34}^{\lambda_{IR}}$ is not null for ragweed, ash and birch pollen. As underlined by (Bickel and Stafford, 1980), this matrix element may be relevant for the study of pollen particles. The diagonal elements are generally larger at wavelength λ_{IR}, which indirectly means easier to evaluate with a higher precision. The considered pollens exhibit a rather pronounced spectral variation except birch for which the matrix elements remain constant within error bars. The spectral dependence however remains complex to interpret, as the scattering matrix elements of pollens depend on the complex refractive index of pollen grains and the literature on pollen refractive indices is rather sparse, with, to our knowledge, no evaluation of their imaginary part and no spectral measurement at wavelengths λ_{VIS} and λ_{IR}.

https://doi.org/10.5194/amt-2021-272
Preprint. Discussion started: 21 September 2021

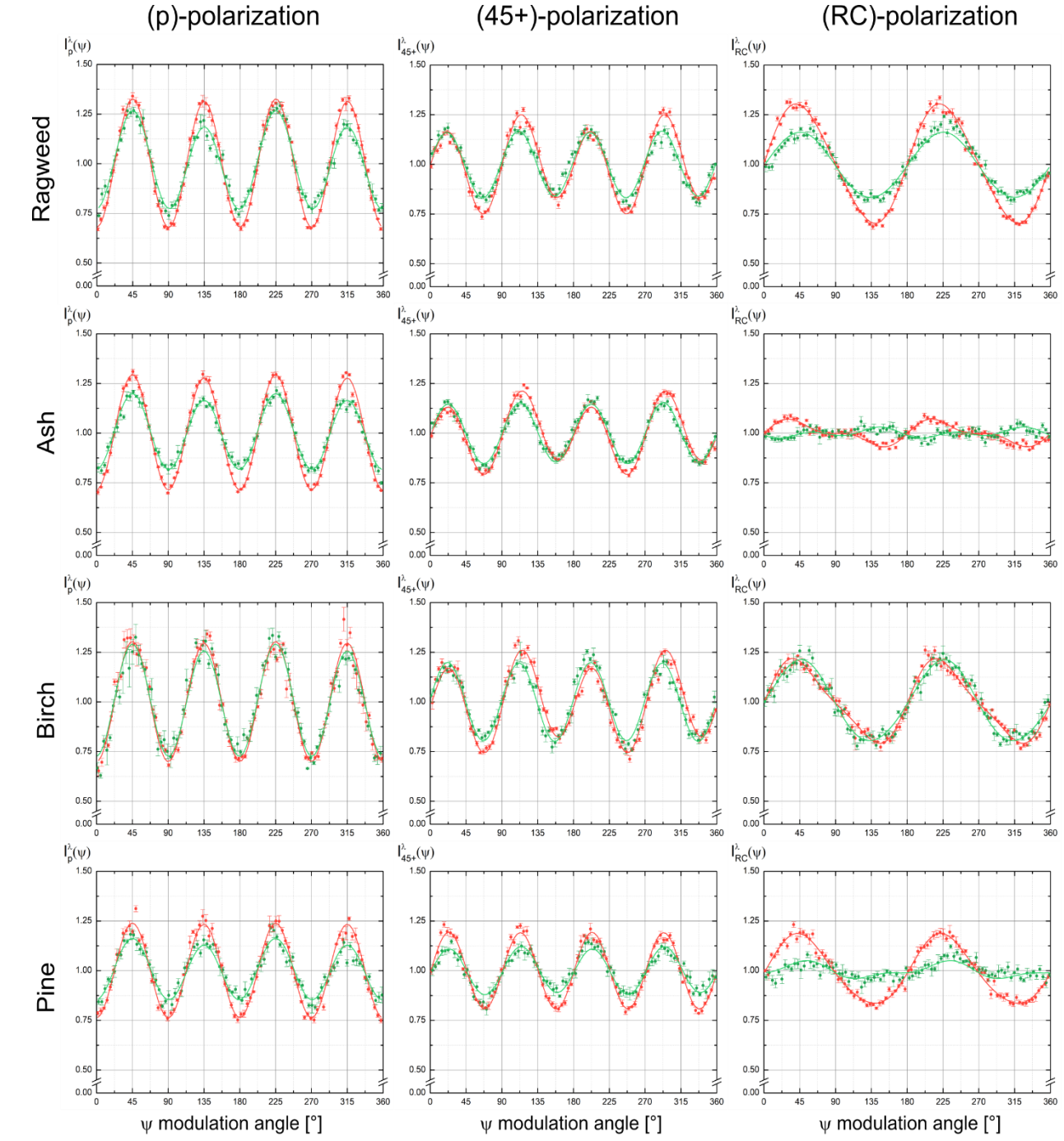

Figure 4: Detected scattered light intensity by ragweed, ash, birch and pine pollens as a function of the of the ψ-angle of the analyser for the three successive incident polarization states (p), (45+) and (RC) at wavelength λ_{VIS} (in green) and wavelength λ_{IR} (in red). The detected light intensity is normalized so that $a_i \times I_0^{\lambda} = 1$, as detailed Section 3.3. A break has been inserted to ease the reading. Each measurement data point is obtained by repeating 400 lasers shots and the uncertainty is calculated by following the methodology described in Section 3.4.

https://doi.org/10.5194/amt-2021-272
Preprint. Discussion started: 21 September 2021

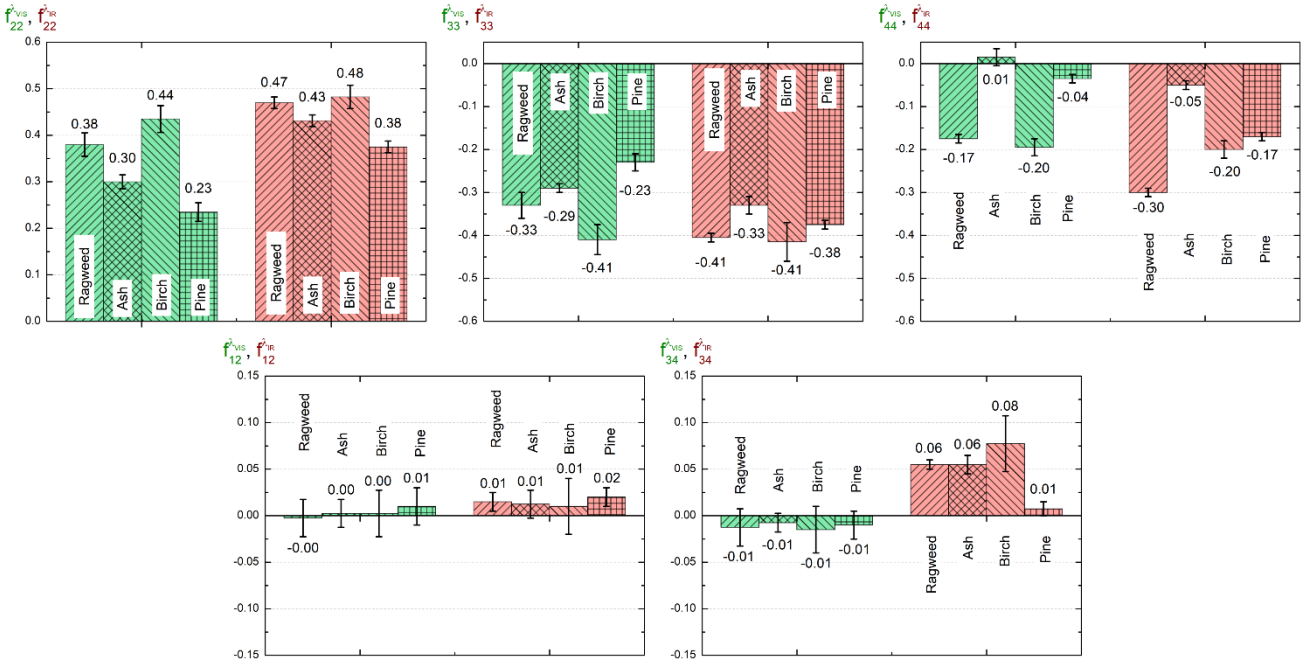

Figure 5: Retrieved scattering matrix elements of ragweed, ash, birch and pine at 177.5° scattering angle at wavelengths λ_{VIS} and λ_{IR}, with corresponding uncertainties evaluated by applying the methodology presented in Section 3. For each pollen taxon, the evaluation of the scattering matrix has been repeated with different samples: each evaluated scattering matrix lies within presented error bars.

Table 1 : Retrieved scattering matrix elements of ragweed, ash, birch and pine at 177.5° scattering angle at wavelength $\boldsymbol{\lambda_{VIS}}$.

Pollen	$f_{22}^{\lambda_{VIS}}$	$f_{33}^{\lambda_{VIS}}$	$f_{44}^{\lambda_{VIS}}$	$f_{12}^{\lambda_{VIS}}$	$f_{34}^{\lambda_{VIS}}$
Ragweed	0.38 ± 0.03	-0.33 ± 0.03	-0.18 ± 0.01	0.00 ± 0.02	-0.01 ± 0.02
Ash	0.30 ± 0.02	-0.29 ± 0.01	0.02 ± 0.02	0.00 ± 0.02	-0.01 ± 0.01
Birch	0.44 ± 0.03	-0.41 ± 0.04	-0.20 ± 0.02	0.00 ± 0.03	-0.02 ± 0.03
Pine	0.24 ± 0.02	-0.23 ± 0.02	-0.04 ± 0.01	0.01 ± 0.02	-0.01 ± 0.02

Table 2: Retrieved scattering matrix elements of ragweed, ash, birch and pine at 177.5° scattering angle at wavelength $\boldsymbol{\lambda_{IR}}$.

Pollen	$f_{22}^{\lambda_{IR}}$	$f_{33}^{\lambda_{IR}}$	$f_{44}^{\lambda_{IR}}$	$f_{12}^{\lambda_{IR}}$	$f_{34}^{\lambda_{IR}}$
Ragweed	0.47 ± 0.01	-0.41 ± 0.01	-0.30 ± 0.01	0.02 ± 0.01	0.06 ± 0.01
Ash	0.43 ± 0.01	-0.33 ± 0.02	-0.05 ± 0.01	0.02 ± 0.02	0.06 ± 0.01
Birch	0.48 ± 0.03	-0.42 ± 0.05	-0.20 ± 0.02	0.01 ± 0.03	0.08 ± 0.03
Pine	0.38 ± 0.01	-0.38 ± 0.01	-0.17 ± 0.01	0.02 ± 0.01	0.01 ± 0.01

https://doi.org/10.5194/amt-2021-272
Preprint. Discussion started: 21 September 2021


Atmospheric Measurement Techniques Discussions

4.3 Towards pollen identification using principal component analysis

As above explained, each of the four considered pollens exhibits its own set of ten scattering elements (five per wavelength), which allow identifying them among the considered set of four pollens. Pine can however be unequivocally identified using $f_{34}^{\lambda_{IR}}$ only as being the only taxon for which $f_{34}^{\lambda_{IR}}$ is null. Also, $f_{22}^{\lambda_{IR}}$ may allow distinguishing pine from other taxa, however not ragweed from birch. Likewise, within our experimental uncertainties, $f_{12}^{\lambda_{VIS}}$ and $f_{34}^{\lambda_{VIS}}$ do not allow differentiating among the four considered pollens. Consequently, for pollen identification through polarized light scattering, the complete set of scattering matrix elements must be generally taken into account, giving rise to the forty elements given in Tables 1 and 2. It however remains challenging and at least non intuitive to identify a pollen taxon based on these set of intricate forty scattering matrix elements. In the literature, decision trees have been applied for classification but overlaps exist due to experimental uncertainties, which limit the application of this classification methodology. Rather, we here propose to reduce the dimensionality of our system to a 2D-representation plane while taking into account experimental uncertainties. Therefore, the goal of this paragraph is to provide a simpler light scattering criterion for classifying among the four considered pollens, based on a 2D-representation plane. To reduce the dimension of our four pollen dataset, a principal component analysis (PCA) has been performed. Indeed, PCA is a statistical method for dimension reduction and feature extraction (Jolliffe, 2005). There, each pollen is described by its two principal components, hereafter called PC_1 and PC_2, which form an orthogonal basis of two uncorrelated components. Each measured scattering pattern can then be defined in terms of a combination of the PCs. Interestingly, besides the advantage of a dimensionality reduction, the PCA maximizes the variance in the (PC_1, PC_2) representation of the dataset. For that, we considered the explained variance, which measures the proportion to which a mathematical model accounts for the dispersion of a given data set. In our case, a threshold of 99 % explained variance is reached by taking into account only two principal components. As a result, Fig. 6 presents the projection of each pollen taxon in the new (PC_1, PC_2)-orthogonal basis. The newly obtained coordinates PC_1 and PC_2 of each pollen account for our ten retrieved scattering matrix elements (five per wavelength per pollen) and the corresponding error bars in Fig. 6 have been evaluated by propagating uncertainties on each f_{ij}^{λ}. The explained variance of PC_1 is 78.8 % while that of PC_2 reaches 20.3 % so that the dimension reduction still accounts for 99.1 % of our experimental variance. Based on Fig. 6, a classification criterion among our four pollen dataset is to assign to each pollen taxon the area delimited by its error bar. To each measured scattering pattern (i.e. each set of ten evaluated f_{ij}^{λ} matrix elements) then corresponds a single point in the (PC_1, PC_2)-basis, which allows identifying the pollen if the evaluated point lies in one of the Fig. 6 coloured areas, which provides a simple criterion for classifying among the four considered pollens, based on a 2D-representation plane. This methodology can interestingly be extended to other pollen taxa provided that precise laboratory measurements of its f_{ij}^{λ} matrix elements are first accurately carried out, as performed in Section 3 for ragweed, ash, birch and pine. Still as is, our methodology allows identifying non equivocal regions in the PCA basis, due to the sensitivity and accuracy of our laboratory work. Hence, our evaluation of pollens

https://doi.org/10.5194/amt-2021-272
Preprint. Discussion started: 21 September 2021

Atmospheric Measurement Techniques Discussions

scattering matrix at two wavelengths, when associated with a principal component analysis, is a step towards identifying non-equivocal polarized light scattering characteristics of pollens, that work for the set of following taxa: ragweed, ash, birch and pine.

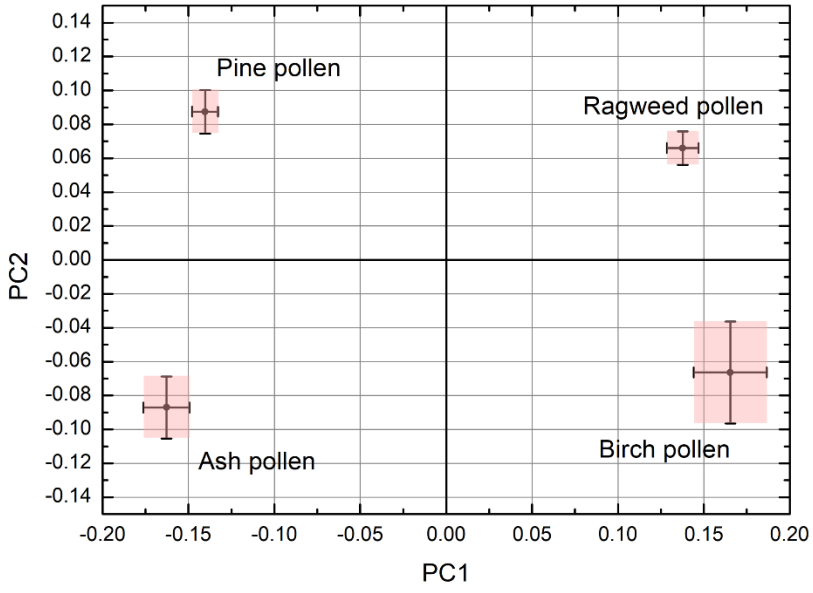

Figure 6: Projection of the ten f_{ij} scattering matrix elements (five per wavelength) for each pollen on the new (PC_1, PC_2)-orthogonal basis using principal component analysis. Error bars have been evaluated by propagating the uncertainties on each f_{ij}^{λ} scattering matrix element. Coloured regions correspond to the range of (PC_1, PC_2) where the pollen taxon can be unequivocally identified among our set of four pollens.

5 Conclusion and outlooks

In a context where pollens are highly impacting atmospheric bioaerosols with a high socio-economical cost, new methodologies are required for monitoring and differentiating pollens. In this paper, the ability of polarized light scattering to differentiate a set of four pollens (ragweed, ash, birch and pine) is experimentally studied in laboratory at two wavelengths. Each pollen taxon having a very specific size and shape, light scattering by these complex-shaped particles is challenging and cannot be easily numerically simulated. In this context, a controlled laboratory experiment, relying on the robust scattering matrix formalism, has been carried out, with special emphasis on the required precision to identify different spectral and polarimetric characteristics of the four considered pollens. This laboratory experiment provides precise retrievals of the scattering matrix elements of each pollen taxon in the form of ten matrix elements (five per wavelength). Hence, a set of ten retrieved matrix elements has been drawn per pollen. Interestingly, within our experimental uncertainties, the four considered pollens, when embedded in ambient air, exhibit clearly different light scattering characteristics, which allowed to differentiate between each pollen taxon from the set of forty matrix elements (five per wavelength per pollen). Finally, to reduce the dimensionality of our system to a 2D-representation plane while taking into account our experimental uncertainties, a principal

https://doi.org/10.5194/amt-2021-272
Preprint. Discussion started: 21 September 2021


Atmospheric Measurement Techniques Discussions

component analysis is here proposed. Though the dimensionality is reduced, this projection of each pollen taxon in the new (PC_1, PC_2)-orthogonal basis interestingly accounts for more than 99 % of our experimental variance, which allow to provide a simple criterion for classifying among the four considered pollens, based on a 2D-representation plane. There are multiple outlooks to this work. To remain focused on laboratory work, which is currently in short supply, the evaluation of the scattering matrix for a larger set of pollens taxon should be considered. If the four chosen pollen taxa are among the most impacting pollens, this work could be extended to other pollens by following our methodology. We may expect our methodology to be applicable to other sets of pollen taxa, provided that the same accuracy is experimentally achieved. The laboratory experiment should then be carried out. As well, extension of this work to other wavelengths, to pollen mixtures, or to other scattering angles is also an interesting outlook of this work.

Author contribution

Danaël Cholleton: Formal analysis, Investigation, Software, Visualization, Writing - original draft, Writing - review & editing. **Emilie Bialic**: Writing - original draft, Project administration. **Antoine Dumas**: Writing - original draft, Project administration. **Pascal Kaluzny**: Project administration, Supervision. **Patrick Rairoux**: Conceptualization, Writing - original draft, Project administration, Supervision. **Alain Miffre**: Conceptualization, Formal analysis, Investigation, Methodology, Supervision, Writing - original draft, Writing - review & editing

Competing interests

The authors declare that they have no conflict of interest.

Acknowledgements

CNRS is acknowledged for financial support and the Lyon Centre Technologique des Microstructures for their help in electronic microscopy.

References

PalDat: https://www.paldat.org/, last access: 21 June 2021.

Bickel, W. S. and Stafford, M. E.: Biological Particles as Irregularly Shaped Scatterers, in: Light Scattering by Irregularly Shaped Particles, Springer, Boston, MA, 299–305, https://doi.org/10.1007/978-1-4684-3704-1_35, 1980.

Biedermann, T., Winther, L., Till, S. J., Panzner, P., Knulst, A., and Valovirta, E.: Birch pollen allergy in Europe, Allergy, 74, 1237–1248, https://doi.org/10.1111/all.13758, 2019.

Bohlmann, S., Filioglou, M., Giannakaki, E., Shang, X., Saarto, A., and Komppula, M.: Characterization of atmospheric pollen with active remote sensing in Finland, in: Geophysical Research Abstracts, 1, 2018.

Cao: Lidar polarization discrimination of bioaerosols, Opt. Eng., 49, 116201, https://doi.org/10.1117/1.3505877, 2010.

Cholleton, D., Bialic, E., Dumas, A., Kaluzny, P., Rairoux, P., and Miffre, A.: Laboratory evaluation of the (VIS, IR) scattering matrix of complex-shaped ragweed pollen particles, J. Quant. Spectrosc. Radiat. Transf., 254, 107223, https://doi.org/10.1016/j.jqsrt.2020.107223, 2020.

Comtois, P., Alcazar, P., and Neron, D.: Pollen counts statistics and its relevance to precision, Aerobiologia, 10, 1999.

Crouzy, B., Stella, M., Konzelmann, T., Calpini, B., and Clot, B.: All-optical automatic pollen identification: Towards an operational system, Atmos. Environ., 140, 202–212, https://doi.org/10.1016/j.atmosenv.2016.05.062, 2016.

Daood, A., Ribeiro, E., and Bush, M.: Pollen Grain Recognition Using Deep Learning, in: Advances in Visual Computing, 321–330, 2016.

Giri, R., Morello, C., Heinson, Y. W., Kemppinen, O., Videen, G., Videen, G., Videen, G., and Berg, M. J.: Generation of aerosol-particle light-scattering patterns from digital holograms, Opt. Lett., 44, 819–822, https://doi.org/10.1364/OL.44.000819, 2019.

Gómez Martín, J. C., Guirado, D., Frattin, E., Bermudez-Edo, M., Cariñanos Gonzalez, P., Olmo Reyes, F. J., Nousiainen, T., Gutiérrez, P. J., Moreno, F., and Muñoz, O.: On the application of scattering matrix measurements to detection and identification of major types of airborne aerosol particles: Volcanic ash, desert dust and pollen, J. Quant. Spectrosc. Radiat. Transf., 271, 107761, https://doi.org/10.1016/j.jqsrt.2021.107761, 2021.

Hamaoui-Laguel, L., Vautard, R., Liu, L., Solmon, F., Viovy, N., Khvorostyanov, D., Essl, F., Chuine, I., Colette, A., Semenov, M. A., Schaffhauser, A., Storkey, J., Thibaudon, M., and Epstein, M. M.: Effects of climate change and seed dispersal on airborne ragweed pollen loads in Europe, Nat. Clim. Change, 5, 766–771, https://doi.org/10.1038/nclimate2652, 2015.

Hesse, M. (Ed.): Pollen terminology: an illustrated handbook, Springer, Wien ; New York, 261 pp., 2009.

Hirst, J. M.: An automatic volumetric spore trap, Ann. Appl. Biol., 39, 257–265, https://doi.org/10.1111/j.1744-7348.1952.tb00904.x, 1952.

Holler, S., Fuerstenau, S. D., and Skelsey, C. R.: Simultaneous two-color, two-dimensional angular optical scattering patterns from airborne particulates: Scattering results and exploratory analysis, J. Quant. Spectrosc. Radiat. Transf., 178, 167–175, https://doi.org/10.1016/j.jqsrt.2016.01.009, 2016.

Imhof, K., Probst, E., Seifert, B., Regenass, S., and Schmid-Grendelmeier, P.: Ash pollen allergy: reliable detection of sensitization on the basis of IgE to Ole e 1, Allergo J. Int., 23, 78–83, https://doi.org/10.1007/s40629-014-0010-8, 2014.

Iwai, T.: Polarization Analysis of Light Scattered by Pollen Grains of *Cryptomeria japonica*, Jpn. J. Appl. Phys., 52, 062404, https://doi.org/10.7567/JJAP.52.062404, 2013.

Jolliffe, I.: Principal Component Analysis, in: Encyclopedia of Statistics in Behavioral Science, American Cancer Society, https://doi.org/10.1002/0470013192.bsa501, 2005.

Kemppinen, O., Laning, J. C., Mersmann, R. D., Videen, G., and Berg, M. J.: Imaging atmospheric aerosol particles from a UAV with digital holography, Sci. Rep., 10, 16085, https://doi.org/10.1038/s41598-020-72411-x, 2020.

Kim, G., Lee, S., Shin, S., and Park, Y.: Three-dimensional label-free imaging and analysis of Pinus pollen grains using optical diffraction tomography, Sci. Rep., 8, https://doi.org/10.1038/s41598-018-20113-w, 2018.

Kiselev, D., Bonacina, L., and Wolf, J.-P.: A flash-lamp based device for fluorescence detection and identification of individual pollen grains, Rev. Sci. Instrum., 84, 033302, https://doi.org/10.1063/1.4793792, 2013.

Lake, I. R., Jones, N. R., Agnew, M., Goodess, C. M., Giorgi, F., Hamaoui-Laguel, L., Semenov, M. A., Solomon, F., Storkey, J., Vautard, R., and Epstein, M. M.: Climate Change and Future Pollen Allergy in Europe, Environ. Health Perspect., 125, 385–391, https://doi.org/10.1289/EHP173, 2017.

Li, Y., Steiner, A., and Solmon, F.: Investigating the direct climatic forcing of pollen and subpollen particles, 2013, A11B-0020, 2013.

Matsuda, S. and Kawashima, S.: Relationship between laser light scattering and physical properties of airborne pollen, J. Aerosol Sci., 124, 122–132, https://doi.org/10.1016/j.jaerosci.2018.07.009, 2018.

Mishchenko, M. I., Travis, L. D., and Lacis, A. A.: Scattering, Absorption, and Emission of Light by Small Particles, Cambridge University Press, 492 pp., 2002.

Mishchenko, M. I., Liu, L., and Videen, G.: Conditions of applicability of the single-scattering approximation, Opt. Express, 15, 7522, https://doi.org/10.1364/OE.15.007522, 2007.

Niederberger, V., Purohit, A., Oster, J. P., Spitzauer, S., Valenta, R., and Pauli, G.: The allergen profile of ash (Fraxinus excelsior) pollen: cross-reactivity with allergens from various plant species, Clin. Exp. Allergy, 32, 933–941, https://doi.org/10.1046/j.1365-2222.2002.01369.x, 2002.

Nouri, S. A., Gregory, D. A., and Fuller, K.: Development of an angle-scanning spectropolarimeter: Preliminary results, J. Quant. Spectrosc. Radiat. Transf., 206, 342–354, https://doi.org/10.1016/j.jqsrt.2017.11.024, 2018.

Pan, Y.-L., Hill, S. C., Pinnick, R. G., House, J. M., Flagan, R. C., and Chang, R. K.: Dual-excitation-wavelength fluorescence spectra and elastic scattering for differentiation of single airborne pollen and fungal particles, Atmos. Environ., 45, 1555–1563, https://doi.org/10.1016/j.atmosenv.2010.12.042, 2011.

Petrov, D.: Photopolarimetrical properties of coronavirus model particles: Spike proteins number influence, J. Quant. Spectrosc. Radiat. Transf., 248, 107005, https://doi.org/10.1016/j.jqsrt.2020.107005, 2020.

Pope, F. D.: Pollen grains are efficient cloud condensation nuclei, Environ. Res. Lett., 5, 044015, https://doi.org/10.1088/1748-9326/5/4/044015, 2010.

Prank, M., Chapman, D. S., Bullock, J. M., Belmonte, J., Berger, U., Dahl, A., Jäger, S., Kovtunenko, I., Magyar, D., Niemelä, S., Rantio-Lehtimäki, A., Rodinkova, V., Sauliene, I., Severova, E., Sikoparija, B., and Sofiev, M.: An operational model for forecasting ragweed pollen release and dispersion in Europe, Agric. For. Meteorol., 182–183, 43–53, https://doi.org/10.1016/j.agrformet.2013.08.003, 2013.

Raman, P., Fuller, K. A., and Gregory, D. A.: Polarization signatures of airborne particulates, Opt. Eng., 52, 074106, https://doi.org/10.1117/1.OE.52.7.074106, 2013.

Sauvageat, E., Zeder, Y., Auderset, K., Calpini, B., Clot, B., Crouzy, B., Konzelmann, T., Lieberherr, G., Tummon, F., and Vasilatou, K.: Real-time pollen monitoring using digital holography, Atmospheric Meas. Tech., 13, 1539–1550, https://doi.org/10.5194/amt-13-1539-2020, 2020.

Schaffner, U., Steinbach, S., Sun, Y., Skjøth, C. A., Weger, L. A. de, Lommen, S. T., Augustinus, B. A., Bonini, M., Karrer, G., Šikoparija, B., Thibaudon, M., and Müller-Schärer, H.: Biological weed control to relieve millions from Ambrosia allergies in Europe, Nat. Commun., 11, 1–7, https://doi.org/10.1038/s41467-020-15586-1, 2020.

Schwendemann, A. B., Wang, G., Mertz, M. L., McWilliams, R. T., Thatcher, S. L., and Osborn, J. M.: Aerodynamics of saccate pollen and its implications for wind pollination, Am. J. Bot., 94, 1371–1381, https://doi.org/10.3732/ajb.94.8.1371, 2007.

Sicard, M., Jorba, O., Ho, J. J., Izquierdo, R., De Linares, C., Alarcón, M., Comerón, A., and Belmonte, J.: Measurement report: Characterization of the vertical distribution of airborne Pinus pollen in the atmosphere with lidar-derived profiles: a modelling case study in the region of Barcelona, NE Spain, Aerosols/Remote Sensing/Troposphere/Physics (physical properties and processes), https://doi.org/10.5194/acp-2021-235, 2021.

https://doi.org/10.5194/amt-2021-272
Preprint. Discussion started: 21 September 2021

Atmospheric Measurement Techniques Discussions

Siljamo, P., Sofiev, M., Filatova, E., Grewling, Ł., Jäger, S., Khoreva, E., Linkosalo, T., Ortega Jimenez, S., Ranta, H., Rantio-Lehtimäki, A., Svetlov, A., Veriankaite, L., Yakovleva, E., and Kukkonen, J.: A numerical model of birch pollen emission and dispersion in the atmosphere. Model evaluation and sensitivity analysis, Int. J. Biometeorol., 57, 125–136, https://doi.org/10.1007/s00484-012-0539-5, 2013.

Smith, M., Cecchi, L., Skjøth, C. A., Karrer, G., and Šikoparija, B.: Common ragweed: A threat to environmental health in Europe, Environ. Int., 61, 115–126, https://doi.org/10.1016/j.envint.2013.08.005, 2013.

Spänkuch, D., Döhler, W., and Güldner, J.: Effect of coarse biogenic aerosol on downwelling infrared flux at the surface, J. Geophys. Res. Atmospheres, 105, 17341–17350, https://doi.org/10.1029/2000JD900173, 2000.

Surbek, M., Esen, C., Schweiger, G., and Ostendorf, A.: Pollen characterization and identification by elastically scattered light, J. Biophotonics, 4, 49–56, https://doi.org/10.1002/jbio.200900088, 2011.

Thibaudon, M., Šikoparija, B., Oliver, G., Smith, M., and Skjøth, C. A.: Ragweed pollen source inventory for France – The second largest centre of Ambrosia in Europe, Atmos. Environ., 83, 62–71, https://doi.org/10.1016/j.atmosenv.2013.10.057, 2014.

Zink, K., Kaufmann, P., Petitpierre, B., Broennimann, O., Guisan, A., Gentilini, E., and Rotach, M. W.: Numerical ragweed pollen forecasts using different source maps: a comparison for France, Int. J. Biometeorol., 61, 23–33, https://doi.org/10.1007/s00484-016-1188-x, 2017.